PHYSICAL REVIEW D **88,** 023001 (2013)

Pulsar interpretation for the AMS-02 result

Peng-Fei Yin, Zhao-Huan Yu, Qiang Yuan, and Xiao-Jun Bi
Key Laboratory of Particle Astrophysics, Institute of High Energy Physics, Chinese Academy of Sciences, Beijing 100049, China
(Received 6 May 2013; published 2 July 2013)

The AMS-02 Collaboration has just published a high-precision measurement of the cosmic positron fraction $e^+/(e^- + e^+)$, which rises with energy from ~5 GeV to ~350 GeV. The result indicates the existence of primary electron/positron sources to account for the positron excess. In this work, we investigate the possibility that the nearby mature pulsars with ages of $O(10^5)$ yr are the primary positron sources. By fitting the data we find that the positrons from a single nearby pulsar, such as Geminga or Monogem, with the spectral index $\alpha \sim 2$ can interpret the AMS-02 result. We also investigate the possibility that high-energy positrons are generated by multiple known pulsars in the ATNF catalogue. Such a scenario can also fit the AMS-02 data well. Future precise measurements of fine structures in the positron spectrum would be a support to the pulsar scenario.

DOI: 10.1103/PhysRevD.88.023001 PACS numbers: 96.50.S−, 97.60.Gb, 98.70.Sa

I. INTRODUCTION

The Alpha Magnetic Spectrometer (AMS-02) Collaboration has just published its first result about the positron fraction in cosmic rays (CRs) measured with an extremely high precision [1]. The positron fraction rises from ~5 GeV continuously up to ~350 GeV, while the slope becomes flat above ~100 GeV. This result is consistent with the PAMELA result about the positron fraction [2,3]. Many studies show that primary electron/positron sources beyond the conventional cosmic ray model are necessary to explain the PAMELA data (see e.g., [4]). Astrophysical sources, like pulsars and pulsar wind nebulae (PWNe) [5–17] or dark matter (DM) annihilation or decay [18–20] have been widely studied as the primary positron sources.

Along the same line, several works have appeared to explain the AMS-02 data [21,22]. DM is still an attractive interpretation. As shown in Ref. [21], DM annihilates into $\tau^+\tau^-$ final states which results in a soft positron spectrum that can account for the AMS-02 data quite well. Other interpretations of DM annihilation or decay into multiple μ or τ leptons may also be fine to reproduce AMS-02 data. The DM annihilation scenarios require a large boost factor and the ''leptophilic'' property of DM particles. However, significant secondary gamma rays are induced by cascade decay, final state radiation, and inverse Compton scattering. Therefore, it is strongly constrained by the Fermi-LAT gamma ray observations from the Galactic center [23,24] or from dwarf galaxies [25,26].

Pulsars are known to be powerful sources in the Galaxy to produce high-energy electrons/positrons with energies of TeV scale or above [27–30]. Primary electrons are extracted from the surface of the pulsar and are accelerated in the magnetosphere by strong electric fields (e.g., 10^{12} V or higher). Energetic curvature radiation is emitted in the strong magnetic field, which will result in electron-positron pairs due to the interactions with magnetic fields or low energy photons. The high energy gamma-ray photons induced by those electron-positron pairs from pulsars have been observed by Fermi-LAT [31].

Unlike the contributions from DM which are assumed to be continuously distributed in the halo and independent of time, the positron injections from pulsars are discrete in the Galactic disk and time-dependent. Since electrons/positrons lose energy quickly via synchrotron radiation and inverse Compton scattering when propagating in the Galaxy, the observed electrons/positrons above ~100 GeV can only come from a small range within a few kpc. A few nearby mature pulsars with ages of $O(10^5)$ yr may have very important contributions to the high-energy electron/positron spectrum and may induce significant deviation from the scenarios with continuous and steady injection.

In this work, we investigate the possibility that nearby mature pulsars are the sources of the observed high energy positions. We use a Markov Chain Monte Carlo (MCMC) method to fit the AMS-02 positron fraction data and determine the model parameters [4]. To determine the properties of the electron backgrounds, we also include the PAMELA electron data [32] in the fit. We consider the possibilities that a single nearby pulsar such as Geminga or Monogem is the source to produce the observed positrons. Through fitting to the data we get the constraints on the parameters of a single pulsar, such as the distance, age, and total injected $e^\pm$ energy. High-energy $e^\pm$ may also be generated by multiple pulsars rather than a certain single pulsar. We then discuss the positron spectrum from a population of pulsars based on the ATNF pulsar catalogue [33]. The multiple pulsars may produce bump like structures in the positron spectrum. We discuss the possibility to distinguish the pulsar and the DM scenarios by a future experiment, such as the Chinese satellite experiment Dark Matter Particle Explorer (DAMPE), which is planned to be launched in 2015 [34].

It is worth emphasizing that the number and the energy distribution of $e^{\pm}$ pairs injected from the pulsar magnetosphere are still open questions. Since there may exist a PWN between the pulsar and the interstellar medium (ISM) (or a supernova remnant), the spectrum of $e^{\pm}$ pairs from the pulsar magnetosphere would be modified by the termination shock and radiation cooling before they are injected into the ISM [13,17]. In comparison with the DM scenario, it is very difficult to obtain a concrete form of the initial $e^{\pm}$ spectrum from pulsar models. Therefore, there would be large uncertainties in the pulsar scenario to explain the high energy positron excesses.

The paper is organized as follows. In Sec. II we describe our treatments for the CR backgrounds and propagation parameters. In Sec. III, we discuss the injection $e^{\pm}$ spectra from the pulsar and their propagations. In Sec. IV, we consider the possibility of a single pulsar as the source of the observed high energy positrons, and take Geminga and Monogem as benchmark examples. In Sec. V, we calculate the positron contributions from multiple pulsars. Then we discuss the possibility to distinguish the pulsar scenario from the DM scenario by a future experiment in Sec. VI. Finally Sec. VII is our conclusion and discussion.

II. COSMIC RAY BACKGROUNDS

The background to explain data includes primary electrons from the CR sources and the secondary positrons/electrons which are generated in the collisions between the CR nuclei and the ISM. In this work, we use the GALPROP code to calculate the background [35,36]. We employ the diffusion reacceleration model for CR propagation. The propagation parameters are adopted by fitting to the boron-to-carbon ratio and unstable-to-stable beryllium ratio [37] (see also [38]). The parameters are $D_0|_{R_0=4\,\mathrm{GV}} = 5.94\times10^{28}\ \mathrm{cm^2\,s^{-1}}$, $\delta = 0.377$, $v_A = 36.4\ \mathrm{km\,s^{-1}}$ and $z_h = 4.04$ kpc. With these propagation parameters, the injection spectrum of the protons is fitted according to the PAMELA [39] and CREAM [40] data. The fitting parameters of the proton injection spectrum are $\nu_1 = 1.80$, $\nu_2 = 2.36$, and $R^p_{\mathrm{br}} = 11.7$ GV, where ν_1 and ν_2 are the spectral indices below and above the break rigidity R^p_{br} [21].

The secondary positrons and electrons can be calculated according to the proton spectrum and the propagation model (see e.g., [41]). To involve some unknown uncertainties, e.g., from the ISM density distribution, the hadronic interactions and the nuclear enhancement factor from the heavy elements, we rescale the calculated fluxes of secondary electrons and positrons with a free factor c_{e^+} in order to fit the data. The range of this factor is adopted to be $0.5 \sim 2$ in the fitting. The injection spectrum of the primary electrons is parametrized by a broken power law with respect to the rigidity (or momentum), $q(R) \propto (R/R^e_{\mathrm{br}})^{-\gamma_1/\gamma_2}$, with γ_1 and γ_2 the indices below and above the break rigidity R^e_{br}. A further normalization factor A_e is needed in the fitting procedure.

For energies less than several tens of GeV, the fluxes of CR particles will be modulated by the solar environment, known as solar modulation. For the positron fraction, the solar modulation effect is less important for $E \gtrsim 10$ GeV. The force field approximation, with only one parameter ϕ, is used to take into account the solar modulation effect [42]. Note the low energy part ($\lesssim$5 GeV) of the positron fraction may not be easily explained with the simple solar modulation model, and more complicated charge-sign dependent modulation is necessary [43,44].

III. HIGH-ENERGY $e^{\pm}$ PAIRS FROM THE PULSAR

The energy of $e^{\pm}$ injected into the ISM is limited by the rotational energy loss rate of the pulsar. The rotational frequency $\Omega = 2\pi/P$, with P the pulse period, decreases as $\dot{\Omega} = -a\Omega^n$. Here $n = \Omega\ddot{\Omega}/\dot{\Omega}^2$ is the breaking index that can be calculated from the measurements of Ω, $\dot{\Omega}$, and $\ddot{\Omega}$. The upper limit of the total $e^{\pm}$ energy is determined by the pulsar spin-down luminosity $\dot{E} = I\Omega|\dot{\Omega}| = a\Omega^{n+1}$, where $I = (2/5)M_sR_s^2$ is the moment of inertia of the pulsar, M_s and R_s are the mass and radius of the pulsar, respectively. For the magnetic dipole radiation the braking index n is equal to 3, and the rotational frequency Ω is given by (see Refs. [5,8] and references therein)

$$\Omega(t) = \Omega_0\left(1 + \frac{t}{\tau_0}\right)^{-1/2}, \tag{1}$$

where Ω_0 is the initial rotational frequency of the pulsar, $\tau_0 = 3c^3I/B_s^2R_s^6\Omega_0^2$ (B_s is the surface magnetic field) is a characteristic time scale describing the spin-down luminosity decays. τ_0 is usually assumed to be $\sim10^4$ year [29]. The spin-down luminosity of a pulsar is then

$$\dot{E}(t) = \frac{I\Omega_0^2}{2\tau_0}\left(1 + \frac{t}{\tau_0}\right)^{-2}. \tag{2}$$

For the pulsar with $t \gg \tau_0$, $\dot{E}$ decreases as t^{-2}. The age of the pulsar T can be obtained through the rotational energy loss rate approximately, $T = \Omega/2|\dot{\Omega}|$. The total energy of electrons and positrons injected from a pulsar is assumed to be proportional to the rotational energy loss, which is

$$E_{\mathrm{out}} = \eta_{e^\pm}\int \dot{E}dt \simeq \eta_{e^\pm}\dot{E}\frac{T^2}{\tau_0}, \tag{3}$$

where $\eta_{e^\pm}$ is the fraction of the rotational energy converted into the energy of electrons and positrons.

The propagation of high energy $e^{\pm}$ can be described by the diffusion equation in the spherically symmetric approximation [28,29]

$$\frac{\partial f}{\partial t} = Q(E,t) + \frac{D(E)}{r^2}\frac{\partial}{\partial r}r^2\frac{\partial f}{\partial r} + \frac{\partial}{\partial E}[b(E)f], \tag{4}$$

where $f(r, t, E)$ is the time-dependent differential density of electrons and positrons (the differential flux is $cf(r, t, E)/4\pi$), $D(E) \propto \beta D_0 (E/E_0)^\delta$ is the diffusion coefficient with D_0 and δ the same as the background calculation (Sec. II). The energy loss rate due to synchrotron and inverse Compton scattering is adopted as $b(E) = b_0 E^2$ with $b_0 = 1.4 \times 10^{-16}$ GeV^{-1} s^{-1} [11].

For the burstlike source, the source term can be taken as a δ function $Q(r, t, E) \propto \delta(r - r_0)\delta(t - t_0)$. This is a good approximation for the pulsar with $T \gg \tau_0$, since most of the rotational energy is lost during the time scale τ_0. The injection energy spectrum of the pulsar is parametrized as a power-law function with an exponential cutoff

$$Q(E, r, t) = Q_0 E^{-\alpha} \exp(-E/E_{\rm cut})\delta(r - r_0)\delta(t - t_0), \tag{5}$$

where α is the spectral index, $E_{\rm cut}$ is the cutoff energy, Q_0 is the normalization factor which can be determined by the total injection energy $E_{\rm out}$. The solution of Eq. (4) for source term Eq. (5) is [28,29]

$$f(d, t_d, E) = \frac{Q_0 E^{-\alpha}}{\pi^{3/2} r_{\rm dif}^3}\left(1 - \frac{E}{E_{\rm max}}\right)^{\alpha-2} \times \exp\left(-\frac{E/E_{\rm cut}}{1 - E/E_{\rm max}} - \frac{d^2}{r_{\rm dif}^2}\right), \tag{6}$$

where d is the distance of the pulsar from the earth and t_d is the diffusion time into the ISM. Note that t_d may be different from the actual age of the pulsar T since electrons and positrons may spend some time in the PWN before their injection in the ISM. Here we simply assume $t_d \approx T$. $E_{\rm max} \simeq (b_0 t_d)^{-1}$ is the maximum energy of electrons and positrons surviving from cooling. For $e^\pm$ with energies larger than $E_{\rm max}$, $f(d, t_d, E)$ is taken to be 0. The diffusion distance $r_{\rm dif}$ is given by

$$r_{\rm dif}(t_d, E) = 2\sqrt{D(E) t_d \frac{1 - (1 - E/E_{\rm max})^{1-\delta}}{(1 - \delta)E/E_{\rm max}}}. \tag{7}$$

Note that for old pulsars with $T \gg 10^5$ yr, the $e^\pm$ injection energy rate is suppressed by $1/T^2$. In addition, the positrons from old pulsars should not contribute much to the observed flux at high energies due to the energy loss in the ISM. The upper limit of the propagation time of the $e^\pm$ with certain energy is

$$t \lesssim \frac{1}{b_0 E} \sim 2.3 \times 10^5 \text{ yr}\left(\frac{E}{\text{TeV}}\right)^{-1}. \tag{8}$$

For young pulsars with $T \leq O(10^4)$ yr, the positrons may not have enough time to propagate to the Earth. Moreover, these positrons may still be trapped in the PWN and not injected in the ISM during such a short time scale. The limit of the propagation time of the $e^\pm$ also suggests an upper limit of the diffusion distance [10],

$$r \lesssim 2\sqrt{D(E)t} \sim 1 \text{ kpc}\left(\frac{E}{\text{TeV}}\right)^{-1/3}. \tag{9}$$

Thus, the nearby pulsars with ages $T \sim O(10^5)$ yr and distances $d \lesssim 1$ kpc are thought to be good candidates to interpret the exotic high-energy positrons.

IV. SINGLE PULSAR

In this section, we study the possibility of using a single pulsar as the high-energy positron source to fit the AMS-02 positron fraction. The background electron spectrum is described by four parameters, i.e., A_e, γ_1, γ_2, $R^e_{\rm br}$, c_{e^+}, and ϕ_e, which are free parameters in our fit. The positron/electron spectrum from pulsars is described by five parameters in Eq. (6), the distance d, the propagation time of t_d, the total injected energy $E_{\rm out}$, the cutoff energy $E_{\rm cut}$, and the spectral index α. For nearby known pulsars, the distance and age are adopted by the ATNF catalogue data. Note that the measurements of the pulsar distance still have some uncertainties. Moreover, the fact that pulsars have velocities of $\sim O(10^2)$ km s^{-1} means that the current distance of the pulsar is different from that during the $e^\pm$ injection period (see e.g., [8] and references therein). Here we do not take into account such uncertainties in our fit.

We consider two nearby pulsars Geminga [J0633 + 1746] with a distance of $d = 0.25$ kpc and age of $T = 3.7 \times 10^5$ yr, and Monogem [B0656 + 14] with $d = 0.28$ kpc and $T = 1.1 \times 10^5$ yr. Here we take the age of the pulsar as the diffusion time. We use a MCMC method to determine $E_{\rm cut}$, α and $E_{\rm tot}$. The resulting positron fraction and electron spectrum for the best fitting parameters for Geminga and Monogem are shown in Fig. 1. The best fitting parameters are given in Table I. From Fig. 1 we can see that the pulsar scenario with these parameters can fit the AMS-02 positron fraction and the PAMELA electron flux data very well.[1] Since Monogem is younger than Geminga, high- energy positrons from Monogem would have smaller energy loss. Thus, the cutoff of the Monogem spectrum is larger than that of Geminga. It is possible to observe such cutoff with more AMS-02 data accumulation.

We also show the confidence regions in the plane of α vs $E_{\rm tot}$ in Fig. 2. Compared with the parameters required to fit the previous PAMELA positron fraction data, the spectrum of the single pulsar becomes softer. The typical injection spectral index for Geminga to interpret the AMS-02 data is in the range of $1.8 \sim 2.1$, while it is ~ 1.5 to fit PAMELA positron fraction data given by Ref. [5]. The observed spin-down luminosity of Geminga is 3.2×10^{34} erg s^{-1}.

[1]Note that here we have considered the low-energy electron data from 1 to 20 GeV in our fit. Since this setting tends to choose a softer spectrum for the electron background, our fit shows a tension between PAMELA and Fermi/HESS electron-positron data. More discussions about this issue can be found in Refs. [21,45].

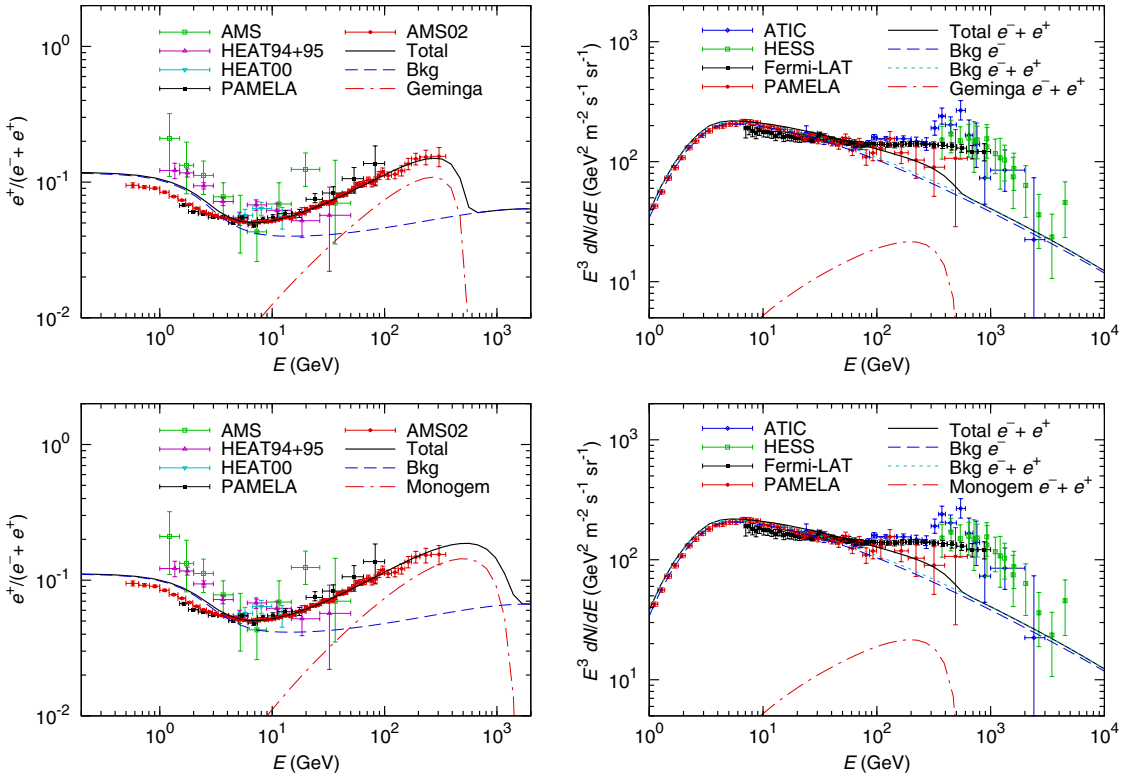

FIG. 1 (color online). The positron fraction (left) and electron flux (right) for the exotic $e^{\pm}$ from Geminga [J0633 + 1746] (upper) and Monogem [B0656 + 14] (lower). Also shown are the positron fraction data from AMS01 [47], HEAT94 + 95 [48], HEAT00 [49], PAMELA [2] and AMS02 [1], and electron flux data from PAMELA [32], ATIC [50], HESS [51,52] and Fermi-LAT [53].

By using Eq. (3) and adopting $\tau_0 = 10^4$ yr, the total injection energy to electron and positron pairs is $1.2\eta_{e^{\pm}} \times 10^{49}$ erg which is comparable with the typical values of our best fit.

A similar conclusion can be applied for Monogem. The typical injection spectrum of Monogem needed to interpret the AMS-02 data has a power-law index within $1.9 \sim 2.2$ which is softer than that for the PAMELA positron data. The observed spin-down luminosity of Monogem is 3.8×10^{34} erg s^{-1}, resulting in the total injection energy $1.48\eta_{e^{\pm}} \times 10^{48}$ erg. The typical value of the $E_{\rm tot}$ in our fit is within $2 \sim 6 \times 10^{48}$ erg.

To relax such an energy tension, one can change the propagation model. Another possibility is that Geminga or Monogem may not be the only source to contribute to the observed high energy positrons.

Then we investigate the correlations between the pulsar distance and age with fixed spectral index and the cutoff energy following [16]. Applying an MCMC method to fit the positron fraction and electron spectrum with $\alpha = 2$ and $E_{\rm cut} = 1$ TeV, we derive the 1σ and 2σ confidence regions in the pulsar parameter space, as shown in Fig. 3.

TABLE I. Parameters of best fit for two nearby pulsars ($E_{\rm cut}$, α and $E_{\rm tot}$) Geminga (with $d = 0.25$ kpc and $T = 3.7 \times 10^5$ yr), Monogem (with $d = 0.28$ kpc and $T = 1.1 \times 10^5$ yr), and electron backgrounds (A_e, γ_1, γ_2, $R^e_{\rm br}$, c_{e^+} and ϕ_e). $R^e_{\rm br}$, $E_{\rm cut}$ and $E_{\rm out}$ are in units of MV, TeV and 10^{48} erg, respectively. A_e is normalized at 1 MeV in unit of cm^{-3} s^{-1} MeV^{-1}.

Pulsar	$E_{\rm cut}$	α	$E_{\rm tot}$	$\log(A_e)$	γ_1	γ_2	$R^e_{\rm br}$	c_{e^+}	ϕ_e
Geminga	1.0	1.98	14.2	−8.93	1.74	2.75	3.61	1.53	720
Monogem	0.62	2.04	3.30	−8.93	1.75	2.75	3.62	1.61	735

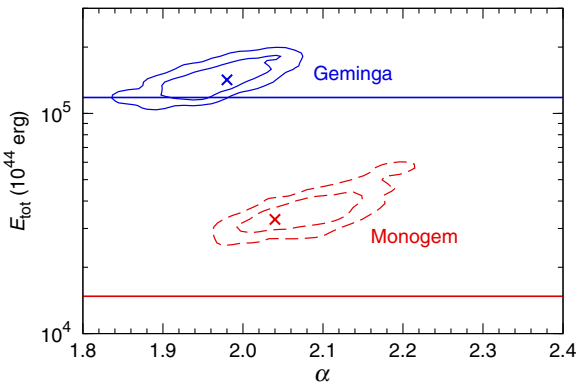

FIG. 2 (color online). 1σ and 2σ confidence regions in the plane of α vs $E_{\rm tot}$ for Geminga (solid contours) and Monogem (dashed contours), respectively. Horizontal lines denote the maximum $E_{\rm out}$ derived by Eq. (3) with $\tau_0 = 10^4$ yr and $\eta_{e^{\pm}} = 1$. Also shown are points for best fits.

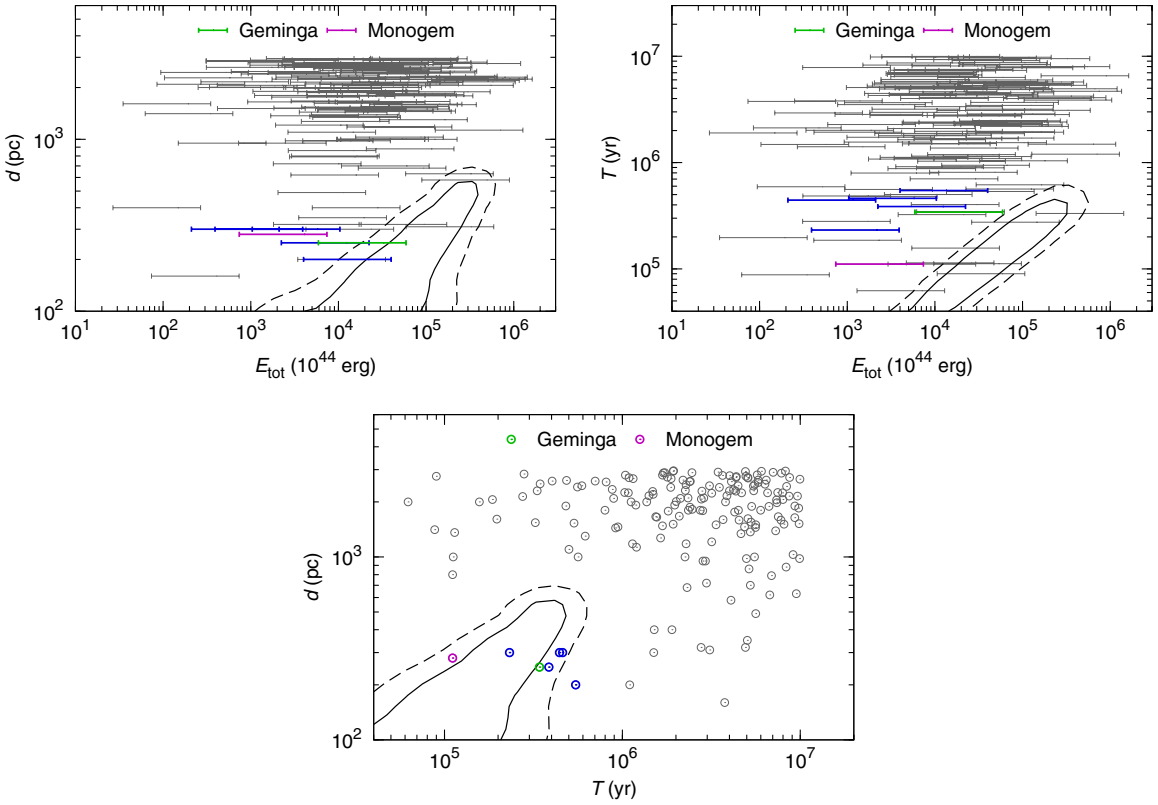

FIG. 3 (color online). 1σ (solid contour) and 2σ (dashed contour) confidence regions in the pulsar parameter space to fit the positron fraction and electron spectrum for $\alpha = 2$ and $E_{cut} = 1$ TeV. The regions are projected onto the E_{tot} vs d (upper left), E_{tot} vs T (upper right), and T vs d (lower) planes. The circles and bars denote the 177 pulsars in the ATNF catalogue within $d < 3$ kpc and $5 \times 10^4 < T(\mathrm{yr}) < 10^7$. E_{tot} for each pulsar is estimated in the range of $5\% \leq \eta_{e^\pm} \leq 50\%$. Seven nearby pulsars with $d < 0.5$ kpc and $T < 10^6$ yr are marked by colors.

In Fig. 3, 177 selected pulsars in the ATNF catalogue with $d < 3$ kpc and $5 \times 10^4 < T(\mathrm{yr}) < 10^7$ are also plotted. E_{tot} for each pulsar is estimated from $\dot{E}$ and T by Eq. (3) with $\tau_0 = 10^4$ yr and $\eta_{e^\pm}$ varying from 5% to 50%. From Fig. 3 we note that the seven nearby pulsars with $d < 0.5$ kpc and $T < 10^6$ yr are more likely to fit the data. We have marked them by colors, with the color green/magenta corresponding to Geminga/Monogem.

Figure 3 shows that the favored region in the pulsar space is rather small. There are several pulsars located near the favored region, especially seven nearby pulsars marked by colors. These pulsars could also have sizable contributions to the high energy $e^\pm$ flux. Therefore, a more reasonable treatment may include the contributions of all suitable pulsars.

V. MULTIPLE PULSARS

It is possible that the flux of high-energy electron/positrons are contributed by many pulsars. Therefore we sum the contribution from all the 177 mature pulsars in the ATNF catalogue to get the positron flux following the method in Ref. [11]. For each pulsar, we randomly assign the parameters in the following ranges: $700 \leq E_{cut}(\mathrm{GeV}) \leq 3000$, $1.5 \leq \alpha \leq 2.3$ and $5\% \leq \eta_{e^\pm} \leq 30\%$. The results are shown in Fig. 4. Obviously, by summing the contributions of all pulsar, even low $e^\pm$ pair conversion efficiency $\eta_{e^\pm}$ could be enough to fit the data.

Since the pulsar parameters vary in large ranges, the resulting total spectrum of all pulsars also varies in a wide band. The energy cutoff of each pulsar depends on the minimum of the injection cutoff E_{cut} and the cooling cutoff E_{max}, and is different from each other. It is further shown that few nearby pulsars could dominate the total flux. Therefore, for each combination of the parameters, the sum spectrum tends to have several bumps at high energies, as shown in Fig. 4.

Since some pulsar radio beams do not point toward the earth, the ATNF catalogue is incomplete. There might be a diffuse population of pulsars which are beyond the observed catalogue. This diffuse component may contribute as another "background" of the electrons/positrons. Similarly as done in [21], we introduce a continuously distributed source component of the diffuse pulsars, with spatial distribution [46]

$$Q(R, z) \propto \left(\frac{R}{R_\odot}\right)^{2.35} \exp\left[-\frac{5.56(R - R_\odot)}{R_\odot}\right] \exp\left(-\frac{|z|}{z_s}\right), \quad (10)$$

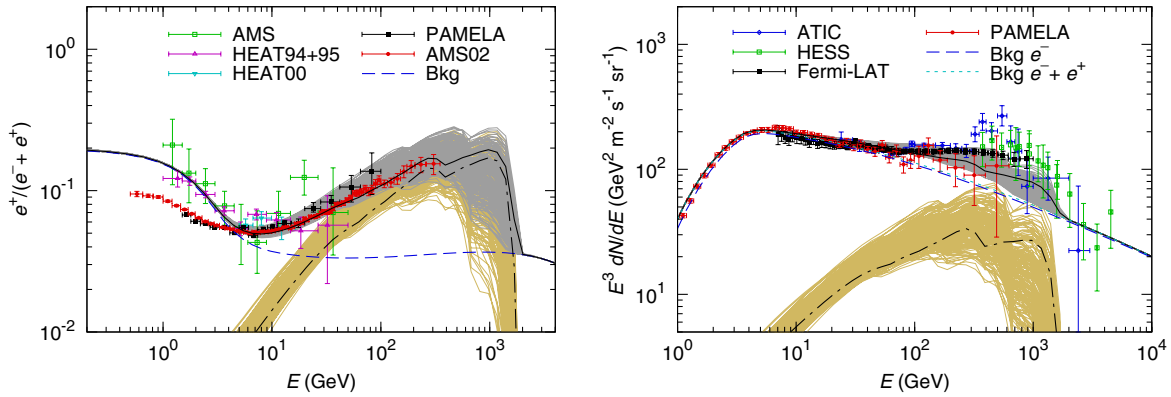

FIG. 4 (color online). The contributions to the positron fraction (left) and electron flux (right) of all the 177 pulsars in the ATNF catalogue with $d < 3$ kpc and $5 \times 10^4 < T(\mathrm{yr}) < 10^7$. The parameters for each pulsar are randomly assigned in the following ranges: $700 \leq E_{\mathrm{cut}}(\mathrm{GeV}) \leq 3000$, $1.5 \leq \alpha \leq 2.3$, and $5\% \leq \eta_{e^\pm} \leq 30\%$. For a particular combination of the parameters, the resulting spectrum including the contributions of all pulsars is represented by a grey line, while a golden line shows only the exotic contributions from the pulsars. A representative choice is shown by black lines (the solid line for the total result, and the dot-dashed line for the exotic contribution).

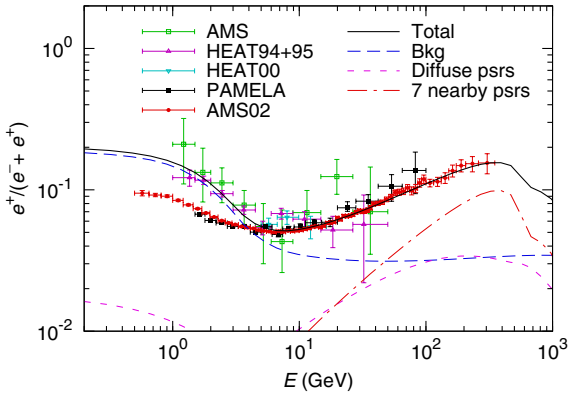

FIG. 5 (color online). Illustration of the positron fraction from both the diffuse pulsars and the seven nearby mature pulsars. The parameters of the seven pulsars are chosen randomly.

where $R_\odot = 8.5$ kpc and $z_s \approx 0.2$ kpc. The energy spectrum of the diffuse pulsars is parametrized by a power-law function with an exponential cutoff.

Figure 5 shows an illustration of the CR positron fraction from both the diffuse pulsars and the seven nearby mature pulsars mentioned above. Here the energy spectrum of the diffuse pulsars is adopted to be proportional to $E^{-2}\exp(-E/600\ \mathrm{GeV})$. The parameters E_{cut}, α, and $\eta_{e^\pm}$ of the seven nearby pulsars are chosen randomly in the ranges described above. Note that only one combination of the parameters is shown in Fig. 5 as an illustration.

VI. DISTINGUISH PULSAR FROM THE DARK MATTER SCENARIO

Both the pulsar and the DM scenarios can fit the AMS-02 data well [21]. It is a fundamental problem to distinguish these two scenarios. As we discussed above if the positron excess is from a few nearby pulsars, it may have a characteristic spectrum with many structures. If such fine structures are discovered, it would be a strong support to the origin of multiple pulsars for the high-energy electrons/positrons. Here we explore the possibility of distinguishing such two scenarios by using future electron/positron spectrum observations. The similar discussions can be found in Refs. [7,9,16].

We generate the mock data using the pulsar set denoted by black dot-dashed line in Fig. 4 as an example, and consider the observation capability of DAMPE. The mock data are produced following the method in Ref. [16]. The number of particles detected in a certain energy bin with a Gaussian energy resolution is given by

$$N(E) = \Delta t \delta E A \int dE' \phi(E') \frac{1}{\sqrt{2\pi\sigma^2}} \exp\left[-\frac{(E'-E)^2}{2\sigma^2}\right], \tag{11}$$

where ϕ is the differential flux, δE is the width of the energy bin, Δt is the observation time, A is the geometrical factor of the detector and σ is determined by $\sigma = \Delta E/2$. ΔE is adopted to be the form of $\Delta E/E = a/\sqrt{E/\mathrm{GeV}} \oplus b$, which is normalized to 1.5% and 10% at 1 TeV and 1 GeV for DAMPE, respectively [34]. The geometrical factor and performing time of the detector are taken to be 0.5 m^2 sr and 5 yr, respectively [34]. The relative statistical uncertainty can be estimated by $\sqrt{N_e}/N_e$. The systematic uncertainty is assumed to be mainly determined by the capability of distinguishing electrons/positrons and other CR particles [16]. Here the e/p separation is taken to be 5×10^5 corresponding to the detector thickness of 32 radiation lengths [34]. The relative systematic uncertainty is estimated by $(N_p/5 \times 10^5)/N_e$.

We use the MCMC method to explore the possible DM parameter space to fit the mock electron/positron flux data for DAMPE, the positron fraction data from AMS-02, and

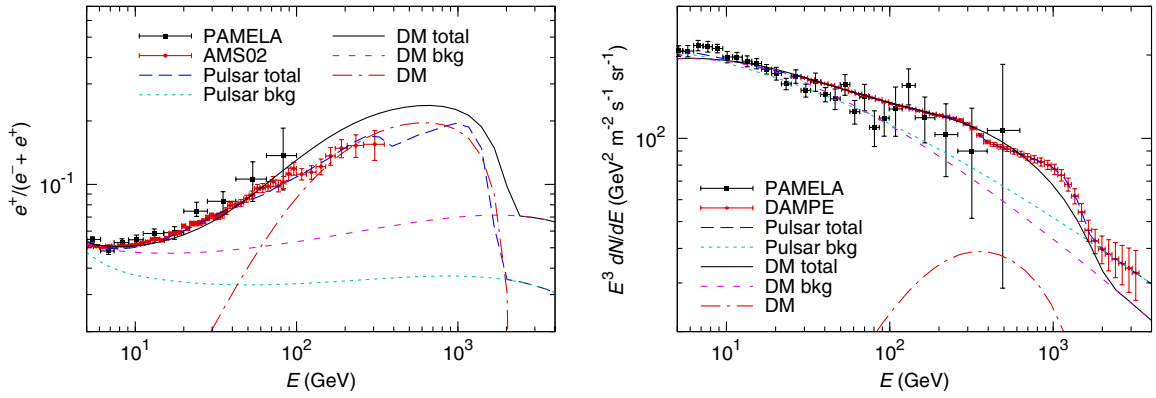

FIG. 6 (color online). The positron fraction (left) and electron flux (right) for the background together with an exotic component from multiple pulsars or DM annihilation in $\tau^+\tau^-$ channel. The "mock" DAMPE data are assumed to be contributed by multiple pulsars and are generated using the pulsar set denoted by black dot-dashed line in Fig. 4. The DM contribution corresponds to the best fit of an MCMC parameter scan.

the electron flux data from PAMELA. As above, the proton injection spectrum is fixed, while the parameters of the primary electron injection spectrum are free. Therefore, the background corresponding to the fit for the DM is usually different with that for multiple pulsars. The DM annihilation final states are taken to be $\tau^+\tau^-$, which induce a soft positron spectrum favored by the AMS-02 result. From the results shown in Fig. 6, we find that the behavior of the electron/postron spectrum from the DM source is mainly determined by the mock DAMPE data below ~300 GeV due to very small uncertainties, and it cannot reproduce the fine structures above 300 GeV at the data. If the differences between the electron/positron spectra from the DM and the pulsar origins are significant as the examples shown here, DAMPE would have the capability to discriminate these two scenarios.

VII. DISCUSSIONS AND CONCLUSIONS

In this work, we investigate the pulsar origin of the positron fraction measured by AMS-02 recently. We first consider the case that the high-energy positrons are produced by a single pulsar, such as Geminga or Monogem. We find the AMS-02 data can be well fitted in this case with a soft power-law injection index of $\alpha \sim 2$. Such a soft spectrum requires a large injection energy from the pulsar, which is comparable to the total energy loss of the pulsar derived from Eq. (3). Considering the uncertainties from CR propagation parameters and the pulsar models, such a tension may be relaxed. We then consider the case that the positrons are from multiple pulsars in the ATNF catalogue. We find such scenario can also fit the AMS-02 data very well.

It is shown that pulsars can be a natural explanation of the AMS-02 positron excess. Compared with the DM scenario, the pulsar scenario may have some distinct features to be distinguished from the DM models. It is very possible that there might be fine structures on the electron/positron spectrum in the pulsar scenario, because the parameters of pulsars might differ from one to another [9]. Furthermore, since one or several nearby pulsar(s) may dominate the flux of high-energy positrons, it may induce a remarkable anisotropy [5,16]. Both the fine structures and the anisotropy could be tested with future observations.

ACKNOWLEDGMENTS

This work is supported by the Natural Science Foundation of China under the Grants No. 11075169, No. 11105155, and No. 11105157 and by the 973 Program under Grant No. 2013CB837000.

Note added.—While this paper was in preparation, two similar papers on the pulsar interpretation for the AMS-02 result appeared [54,55]. Our results for fitting the AMS-02 data are consistent with theirs.

[1] M. Aguilar *et al.* (AMS Collaboration), Phys. Rev. Lett. **110**, 141102 (2013).
[2] O. Adriani *et al.* (PAMELA Collaboration), Nature (London) **458**, 607 (2009).
[3] O. Adriani, G. C. Barbarino, G. A. Bazilevskaya, R. Bellotti, M. Boezio, E. A. Bogomolov, L. Bonechi, M. Bongi, V. Bonvicini, and S. Borisov, Astropart. Phys. **34**, 1 (2010).
[4] J. Liu, Q. Yuan, X.-J. Bi, H. Li, and X. Zhang, Phys. Rev. D **85**, 043507 (2012).
[5] D. Hooper, P. Blasi, and P. D. Serpico, J. Cosmol. Astropart. Phys. 01 (2009) 025.

[6] H. Yuksel, M. D. Kistler, and T. Stanev, Phys. Rev. Lett. **103**, 051101 (2009).
[7] J. Hall and D. Hooper, Phys. Lett. B **681**, 220 (2009).
[8] S. Profumo, Central Eur. J. Phys. **10**, 1 (2012).
[9] D. Malyshev, I. Cholis, and J. Gelfand, Phys. Rev. D **80**, 063005 (2009).
[10] N. Kawanaka, K. Ioka, and M. M. Nojiri, Astrophys. J. **710**, 958 (2010); N. Kawanaka, Nucl. Instrum. Methods Phys. Res., Sect. A **630**, 52 (2011).
[11] D. Grasso *et al.* (FERMI-LAT Collaboration), Astropart. Phys. **32**, 140 (2009).
[12] T. Delahaye, J. Lavalle, R. Lineros, F. Donato, and N. Fornengo, Astron. Astrophys. **524**, A51 (2010).
[13] P. Blasi and E. Amato, arXiv:1007.4745.
[14] K. Kashiyama, K. Ioka, and N. Kawanaka, Phys. Rev. D **83**, 023002 (2011).
[15] T. Kamae, S.-H. Lee, L. Baldini, F. Giordano, M.-H. Grondin, L. Latronico, M. Lemoine-Goumard, C. Sgro *et al.*, arXiv:1010.3477.
[16] M. Pato, M. Lattanzi, and G. Bertone, J. Cosmol. Astropart. Phys. 12 (2010) 020.
[17] P. D. Serpico, Astropart. Phys. **39–40**, 2 (2012).
[18] L. Bergstrom, T. Bringmann, and J. Edsjo, Phys. Rev. D **78**, 103520 (2008); V. Barger, W. Y. Keung, D. Marfatia, and G. Shaughnessy, Phys. Lett. B **672**, 141 (2009); I. Cholis, L. Goodenough, D. Hooper, M. Simet, and N. Weiner, Phys. Rev. D **80**, 123511 (2009); M. Cirelli, M. Kadastik, M. Raidal, and A. Strumia, Nucl. Phys. **B813**, 1 (2009); **B873**, 530(E) (2013); N. Arkani-Hamed, D. P. Finkbeiner, T. R. Slatyer, and N. Weiner, Phys. Rev. D **79**, 015014 (2009); M. Pospelov and A. Ritz, Phys. Lett. B **671**, 391 (2009); P. J. Fox and E. Poppitz, Phys. Rev. D **79**, 083528 (2009).
[19] P.-f. Yin, Q. Yuan, J. Liu, J. Zhang, X.-j. Bi, S.-h. Zhu, and X.-m. Zhang, Phys. Rev. D **79**, 023512 (2009); K. Ishiwata, S. Matsumoto, and T. Moroi, Phys. Lett. B **675**, 446 (2009); A. Ibarra and D. Tran, J. Cosmol. Astropart. Phys. 02 (2009) 021; C.-R. Chen, M. M. Nojiri, F. Takahashi, and T. T. Yanagida, Prog. Theor. Phys. **122**, 553 (2009); A. Arvanitaki, S. Dimopoulos, S. Dubovsky, P. W. Graham, R. Harnik, and S. Rajendran, Phys. Rev. D **79**, 105022 (2009).
[20] Y.-Z. Fan, B. Zhang, and J. Chang, Int. J. Mod. Phys. D **19**, 2011 (2010); M. Cirelli, Pramana **79**, 1021 (2012).
[21] Q. Yuan, X.-J. Bi, G.-M. Chen, Y.-Q. Guo, S.-J. Lin, and X. Zhang, arXiv:1304.1482.
[22] J. Kopp, arXiv:1304.1184; A. De Simone, A. Riotto, and W. Xue, J. Cosmol. Astropart. Phys. 05 (2013) 003; M. Ibe, S. Iwamoto, S. Matsumoto, T. Moroi, and N. Yokozaki, arXiv:1304.1483; H.-B. Jin, Y.-L. Wu, and Y.-F. Zhou, arXiv:1304.1997; Y. Kajiyama, H. Okada, and T. Toma, arXiv:1304.2680.
[23] X.-Y. Huang, Q. Yuan, P.-F. Yin, X.-J. Bi, and X.-L. Chen, J. Cosmol. Astropart. Phys. 11 (2012) 048.
[24] D. Hooper, C. Kelso, and F. S. Queiroz, arXiv:1209.3015.
[25] A. A. Abdo *et al.* (Fermi-LAT Collaboration), Astrophys. J. **712**, 147 (2010).
[26] Y.-L. S. Tsai, Q. Yuan, and X. Huang, J. Cosmol. Astropart. Phys. 03 (2013) 018.
[27] P. Goldreich and W. H. Julian, Astrophys. J. **157**, 869 (1969).
[28] F. A. Aharonian, A. M. Atoyan, and H. J. Volk, Astron. Astrophys. **294**, L41 (1995).
[29] A. M. Atoian, F. A. Aharonian, and H. J. Volk, Phys. Rev. D **52**, 3265 (1995).
[30] L. Zhang and K. S. Cheng, Astron. Astrophys. **368**, 1063 (2001).
[31] A. A. Abdo *et al.* (Fermi LAT Collaboration), Astrophys. J. Suppl. Ser. **187**, 460 (2010); **193**, 22(E) (2011).
[32] O. Adriani *et al.* (PAMELA Collaboration), Phys. Rev. Lett. **106**, 201101 (2011).
[33] R. N. Manchester, G. B. Hobbs, A. Teoh, and M. Hobbs, Astron. J. **129**, 1993 (2005).
[34] J. Chang, in Proceedings of DSU 2011 Conference, 2011 (to be published).
[35] I. V. Moskalenko and A. W. Strong, Astrophys. J. **493**, 694 (1998).
[36] A. W. Strong and I. V. Moskalenko, Astrophys. J. **509**, 212 (1998).
[37] S. J. Lin *et al.* (unpublished).
[38] T. Delahaye, R. Lineros, F. Donato, N. Fornengo, and P. Salati, Phys. Rev. D **77**, 063527 (2008).
[39] O. Adriani *et al.* (PAMELA Collaboration), Science **332**, 69 (2011).
[40] H. S. Ahn, P. Allison, M. G. Bagliesi, J. J. Beatty, G. Bigongiari, J. T. Childers, N. B. Conklin, S. Coutu *et al.*, Astrophys. J. **714**, L89 (2010).
[41] T. Delahaye, F. Donato, N. Fornengo, J. Lavalle, R. Lineros, P. Salati, and R. Taillet, Astron. Astrophys. **501**, 821 (2009).
[42] L. J. Gleeson and W. I. Axford, Astrophys. J. **154**, 1011 (1968).
[43] S. Della Torre, P. Bobik, M. J. Boschini, C. Consolandi, M. Gervasi, D. Grandi, K. Kudela, S. Pensotti *et al.*, Adv. Space Res. **49**, 1587 (2012).
[44] L. Maccione, Phys. Rev. Lett. **110**, 081101 (2013).
[45] Q. Yuan and X.-J. Bi, arXiv:1304.2687.
[46] D. R. Lorimer, arXiv:astro-ph/0308501.
[47] M. Aguilar *et al.* (AMS-01 Collaboration), Phys. Lett. B **646**, 145 (2007).
[48] S. W. Barwick *et al.* (HEAT Collaboration), Astrophys. J. **482**, L191 (1997).
[49] S. Coutu *et al.*, in *Proceedings of International Cosmic Ray Conference* (American Institute of Physics, New York, 2001), Vol. 5, p. 1687.
[50] J. Chang, J. H. Adams, H. S. Ahn, G. L. Bashindzhagyan, M. Christl, O. Ganel, T. G. Guzik, J. Isbert *et al.*, Nature (London) **456**, 362 (2008).
[51] F. Aharonian *et al.* (H.E.S.S. Collaboration), Phys. Rev. Lett. **101**, 261104 (2008).
[52] F. Aharonian *et al.* (H.E.S.S. Collaboration), Astron. Astrophys. **508**, 561 (2009).
[53] M. Ackermann *et al.* (Fermi LAT Collaboration), Phys. Rev. D **82**, 092004 (2010).
[54] T. Linden and S. Profumo, arXiv:1304.1791.
[55] I. Cholis and D. Hooper, arXiv:1304.1840.